

RESEARCH LETTER

10.1002/2017GL076634

Key Points:

- Individual magnetic moments are isolated for a suite of grains while embedded in a nonmagnetic medium using micromagnetic tomography
- The traditional nonuniqueness of this inversion problem is tackled by adding spatial information using microCT scanning
- Our new technique is nondestructive; hence, grains can be analyzed multiple times and in different magnetic states

Supporting Information:

- Supporting Information S1

Correspondence to:

L. V. de Groot,
l.v.degroot@uu.nl

Citation:

de Groot, L. V., Fabian, K., Béguin, A., Reith, P., Barnhoorn, A., & Hilgenkamp, H. (2018). Determining individual particle magnetizations in assemblages of micrograins. *Geophysical Research Letters*, 45, 2995–3000. <https://doi.org/10.1002/2017GL076634>

Received 1 DEC 2017

Accepted 18 MAR 2018

Accepted article online 26 MAR 2018

Published online 6 APR 2018

©2018. The Authors.

This is an open access article under the terms of the Creative Commons Attribution-NonCommercial-NoDerivs License, which permits use and distribution in any medium, provided the original work is properly cited, the use is non-commercial and no modifications or adaptations are made.

Determining Individual Particle Magnetizations in Assemblages of Micrograins

Lennart V. de Groot¹ , Karl Fabian² , Annemarieke Béguin¹ , Pim Reith³ , Auke Barnhoorn⁴ , and Hans Hilgenkamp³ 

¹Paleomagnetic laboratory Fort Hoofddijk, Faculty of Geosciences, Utrecht University, Utrecht, Netherlands, ²NGU, Geological Survey of Norway, Trondheim, Norway, ³MESA+ Institute for Nanotechnology, University of Twente, Enschede, Netherlands, ⁴Department of Geoscience and Engineering, Faculty of Civil Engineering and Geosciences, Delft University of Technology, Delft, Netherlands

Abstract Obtaining reliable information from even the most challenging paleomagnetic recorders, such as the oldest igneous rocks and meteorites, is paramount to open new windows into Earth's history. Currently, such information is acquired by simultaneously sensing millions of particles in small samples or single crystals using superconducting quantum interference device magnetometers. The obtained rock-magnetic signal is a statistical ensemble of grains potentially differing in reliability as paleomagnetic recorder due to variations in physical dimensions, chemistry, and magnetic behavior. Here we go beyond bulk magnetic measurements and combine computed tomography and scanning magnetometry to uniquely invert for the magnetic moments of individual grains. This enables us to select and consider contributions of subsets of grains as a function of particle-specific selection criteria and avoid contributions that arise from particles that are altered or contain unreliable magnetic carriers. This new, nondestructive, method unlocks information from complex paleomagnetic recorders that until now goes obscured.

Plain Language Summary Information about the past state of the Earth's magnetic field is obtained from igneous rocks that take a snapshot of the ambient magnetic field as they cool. Igneous rocks, however, contain a broad range of different grains that have their specific magnetic properties, and many are known to be incapable of storing a magnetization reliably over time. The signal obtained from traditional bulk samples that contain many millions of grains is a statistical ensemble of all these grains—the good and the bad. To improve the quality of the magnetic signal from these rocks, we go beyond bulk samples and identify magnetizations of individual grains in a sample using an X-ray tomography-assisted magnetic inversion. We show that it is possible to uniquely and nondestructively obtain magnetizations for a limited number of grains. Isolating the individual magnetizations of grains enables selecting only the known good recorders and rejecting the adverse recorders present in the sample. This would make it possible to obtain information from even the most complex paleomagnetic recorders, including igneous rocks, meteorites, and extraterrestrial material that until now goes obscured.

1. Introduction

Thermoremanent magnetizations (TRMs) of assemblages of magnetic particles in geological materials or archeological artifacts are the primary recorders of the direction and intensity of the ancient geomagnetic field. TRMs provide information about, for example, the early Earth's magnetopause standoff (Tarduno et al., 2010), the Earth's inner core formation (Biggin et al., 2015), and regional, rapid variations in the Earth's magnetic field (de Groot et al., 2013). Iron oxides like magnetite record the Earth's magnetic field by acquiring a TRM as they cool through their Curie and subsequent blocking temperature. For small, single-domain grains, the acquisition and preservation of magnetic signals are physically underpinned by Néel's theory (Néel, 1949, 1955), based on statistics of individual magnetic moments. In practice, the dominantly occurring larger multidomain (MD) iron oxides violate Néel's theory and lead to unstable magnetizations caused by, for example, viscous reordering of magnetic domains (de Groot et al., 2014). Moreover, the magnetic particles in natural samples vary in chemical composition, size, and shape and differ substantially in their magnetic recording properties; the bulk magnetic signal is a statistical ensemble representing all these recorders—the good and the bad.

Many studies have employed high-end magnetometry techniques to go beyond the traditional bulk rock measurements to unravel the magnetic state of Earth materials and meteorites or to progress our fundamental knowledge of micromagnetic processes in MD grains. Recent examples are electron holography (Almeida et al., 2014), scanning superconducting quantum interference device microscopy (SSM) (Lima & Weiss, 2009; Weiss et al., 2007), magnetic tunnel junction scanners (Lima et al., 2014), X-ray photoemission electron microscopy (Nichols et al., 2016), and quantum diamond microscopes (Farchi et al., 2017; Glenn et al., 2017). Some of these studies tried to avoid the adverse contribution of bad paleomagnetic recorders by selecting the most suitable materials or the best regions in a sample, but none attempted to obtain magnetic information for individual magnetic grains. If we would be able to isolate the magnetic moments of individual grains, we could select the best recorders and derive the paleomagnetic information directly from them, (mathematically) avoiding the adverse contribution of bad recorders. Ideally, paleomagnetic information would be obtained by distinguishing signals from $>10^6$ individual magnetic particles and averaging their magnetization vectors over systematically chosen coercivity classes of reliable magnetization carriers (Berndt et al., 2016). This is currently beyond reach, partly because of insufficient nanometer-scale measurement techniques and partly because of the nonuniqueness of magnetic inversion.

Here we show that the magnetic moments of a number of individual particles embedded in a nonmagnetic matrix can be uniquely and nondestructively determined by combining information on the spatial characteristics of the remanence carrying grains and scans of the magnetic flux density on the surface of the sample. As the techniques used are nondestructive, samples can be analyzed multiple times and in different magnetization states. This enables characterizing changes between magnetizations and the magnetic stability of individual grains.

2. Materials and Methods

To control the dispersion and grain-size distribution of magnetic particles in a nonmagnetic matrix we created a synthetic sample. Magnetite grains of natural origin (Hartstra, 1982) with diameters ranging from 5 to 35 μm were cast in epoxy at $\sim 2,800$ grains per cubic millimeter, approximately 1 order of magnitude less dense than in natural samples. This suite of grain sizes represents an important segment of the dominant rock-magnetic carriers in igneous rocks that are often used for paleointensity experiments. The sizes, shapes, and locations of these grains were determined by X-ray computed tomography (microCT imaging). This technique produces a three-dimensional density distribution of the sample (Sakellariou et al., 2004). As the density of iron oxides is much higher than the densities of other naturally occurring minerals and epoxy, the spatial characteristics of the grains of interest can be determined and are outlined by groups of voxels (Figure 1a); the largest grains are described by $\sim 80,000$ voxels.

The component of the magnetic flux density perpendicular to the polished surface of the sample is assessed by SSM (Kirtley & Wikswo, 1999). The tip of the sensor is in contact with the sample; hence, the distance between the sample surface and the pickup loop is $\sim 2 \mu\text{m}$. The diameter of the sensor is 3 μm , but the effective area of the sensor is increased to $\sim 21 \mu\text{m}^2$ due to flux focusing by the superconducting Niobium pickup loop. Each measurement is therefore an average over this effective area; this effect inherently smooths gradients in the flux density maps. As the step size used for the SSM scanning is 1 μm , each grid point is measured 21 times. This oversampling of the magnetic flux density is considered in the geometry of the inversion model and increases the signal-to-noise ratio considerably (Figure 1b).

Because the SSM sensor is in contact with the sample both the sample and the sensor are submerged in liquid helium; hence the measurements were done at $T = 4 \text{ K}$, below the Verwey transition of magnetite. The nature of the remanent magnetizations in our grains is not exactly known and could be a TRM. TRMs generally broadly compare to anhysteretic remanent magnetizations (ARMs) in terms of magnetic behavior; for ARMs the effect of the Verwey transition is a $\sim 15\%$ decrease in magnetization (Muxworthy et al., 2003), which is almost reversible; changes in direction are not expected (Muxworthy & McClelland, 2000). After the first SSM scan that was done on an untreated, hence magnetically randomized sample, an asymmetrical alternating field (40 μT bias field superimposed on a 300 mT alternating field) under an angle of 45° with respect to the surface was applied to impart a new ARM state on the sample, which then was assessed by a second SSM scan.

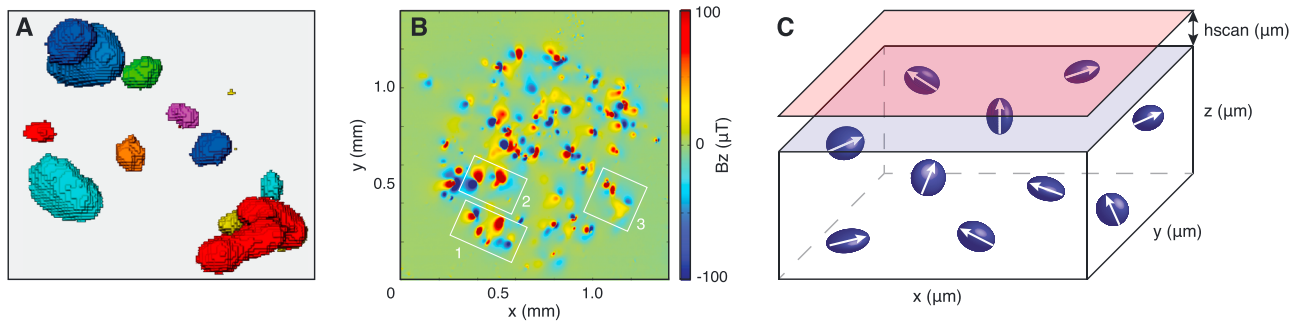


Figure 1. The rationale of micromagnetic tomography. The sizes, shapes, and locations of the grains are described by groups of voxels obtained by microCT scanning (a); different colors indicate individual grains. The map of the normal component of the magnetic flux density (b) is produced by scanning superconducting quantum interference device microscopy; the three areas used in this study are within the white outlines. The measured flux density in the plane at distance “hscan” above the sample can be inverted onto the spatial definitions of the grains to determine the magnetization of individual grains in the medium (c).

The SSM and microCT results are mapped using the grains closest to the surface: the center of their magnetic expression on the surface is placed on top of the grains in the microCT data (Figure 1c). Both data sets together yield a unique and robust inversion of the surface magnetic flux densities that produces individual particle magnetizations of a (sub)set of iron oxide grains.

The individual magnetic moments are obtained by performing a pseudoinverse of a matrix populated with the total magnetic flux through the sensor loop that arises from particles identified as iron oxides for each point in the SSM scan. The magnetic flux through the sensor loop generated by homogeneously magnetized cuboids is described by a forward calculation of the SSM signal using analytical integrals (Figures 1c and S2 in the supporting information). The total SSM signal can be obtained by adding all signals from iron oxide voxels where voxels from the same grain carry the same magnetization. This is accelerated by a factor of 10–100 by grouping voxels into larger cuboids such that the exact shape of the grain is rebuilt by adding at each step the largest possible cuboid that fits in the residual volume left by the previous cuboids (Figure S3).

The number of individual, magnetized grains is obtained through microCT; for K particles $3K$ magnetization variables $M_{1,x}, M_{1,y}, M_{1,z}, \dots, M_{K,x}, M_{K,y}, M_{K,z}$ have to be determined. That the resulting specific inversion problem has a unique solution can be certified by finding a subset of $3K$ SSM data points for which the forward matrix is invertible. If such a subset can be found, it proves that no second different assignment $M'_{1,x}, M'_{1,y}, M'_{1,z}, \dots, M'_{K,x}, M'_{K,y}, M'_{K,z}$ exists that leads to the same measurement values. The microCT particle localization in these cases resolves the nonuniqueness inherent to common potential field inversions, where

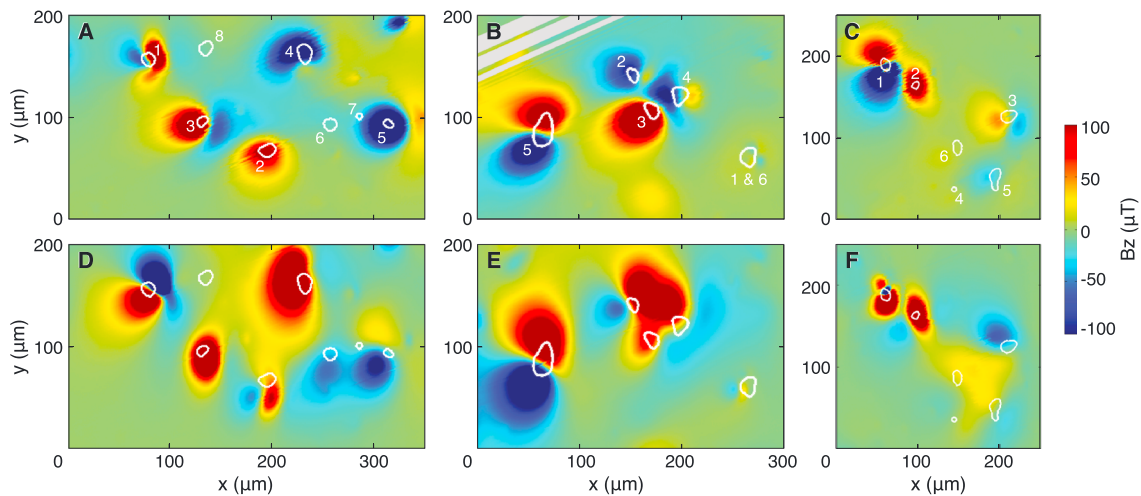


Figure 2. Scanning superconducting quantum interference device microscopy (SSM) results of the three areas subjected to the inversion. The SSM results of area 1 (a), 2 (b), and 3 (c) of the sample in unknown magnetic state; the white outlines are the locations of the grains; the numbers refer to grains in the text and Table S2 and increase with depth of the grain. Some bad traces were removed from area 2 (b, gray lines). The SSM results for the sample in the anhyseretic remanent magnetization state are given for area 1 (d), 2 (e), and 3 (f) with the same outlines of the grains.

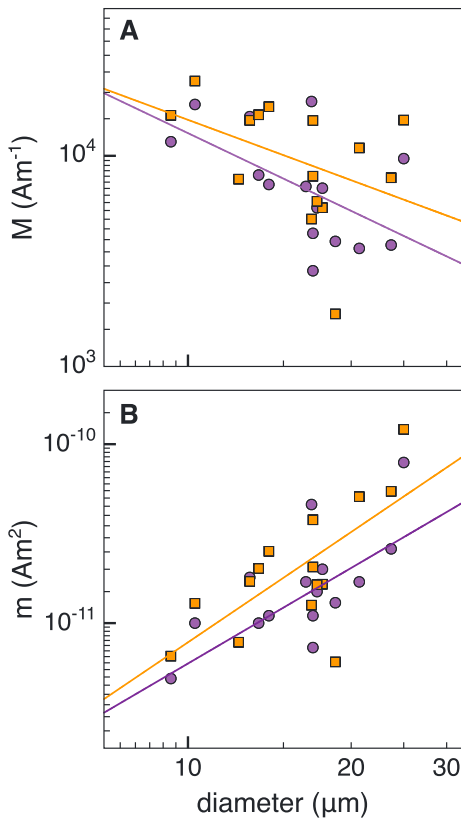


Figure 3. The relation between grain diameter and magnetization (a) and magnetic moment (b). The grains in their anhysteretic remanent magnetization state (orange) have larger magnetizations than the grains in the random magnetic state (purple) but for both the volume magnetizations decrease with grain size (a). This trend is mitigated by the inherent increase in volume with increasing diameter, as the total magnetic moment of the grain increases with diameter (b).

such certification is not possible. The full inversion of all $P > 3$ K SSM measurements is then performed via the pseudoinverse of the $3 K \times P$ forward matrix in order to reduce the influence of measurement noise. A mathematical theorem that guarantees uniqueness of tomography-assisted inversion in a much more general setting is in progress (Fabian & de Groot, 2017).

3. Results

Three small areas of up to 200 by 350 μm containing up to eight grains each are considered independently in both magnetic states (Figures 2a–2f). Solving the inversion for smaller areas makes the inversion computationally feasible. Furthermore, the mapping between the SSM and microCT data is improved as minor distortions between these two data sets are suppressed by optimizing the mapping per area. The three areas together contain 20 grains; the obtained volume normalized magnetizations range from 0.4 to 92.2, with a median value of 7.1 kA/m for the initial magnetic state and range from 0.4 to 132.0 with a median value of 9.5 kA/m in the ARM state. For both states the directions seem randomly distributed; however, the magnetic moments of the individual grains changed considerably between the two scans, both in direction and in magnitude (Table S2).

The magnetizations of the grains in the first scan are random; for example, the grains could still hold an old remanence or—more likely—became magnetized in the process of sample preparation. Imparting a new ARM in the sample increased the magnetization of each individual grain on average by 77%. For both magnetic states the magnetization of the grains decreases with grain size (Figure 3a). This decrease, however, is negated by the inherent increase in volume for grains with a larger diameter; that is, the magnetic moment of a grain with a diameter of 30 μm is approximately 1 order of magnitude

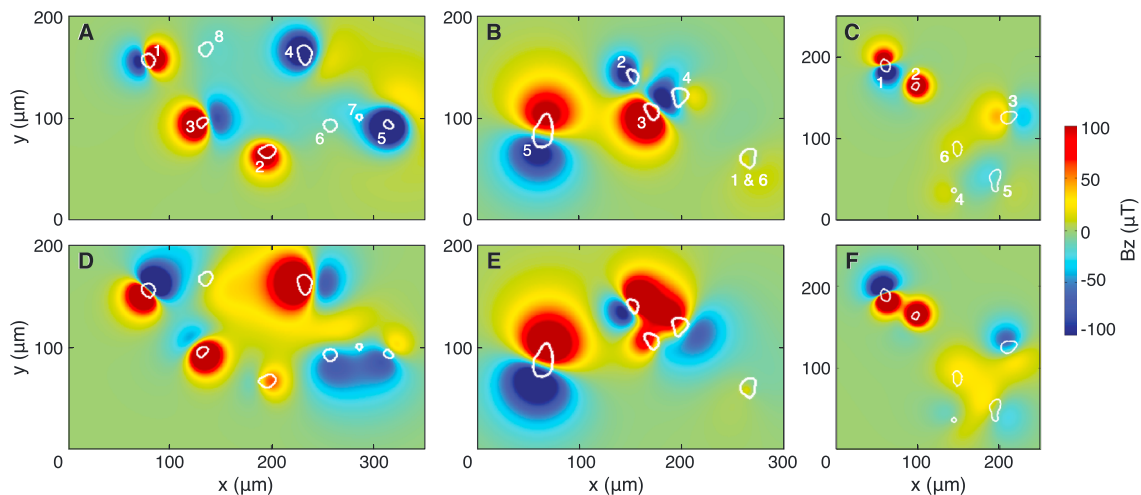


Figure 4. Calculated magnetic flux density normal to the surface of the sample given the inverted magnetic moments and the sizes, shapes, and locations of the grains. The results of area 1 (a), 2 (b), and 3 (c) of the sample in unknown magnetic state; the white outlines are the locations of the grains; the numbers refer to grains in the text and Table S2. The results for the sample in the ARM state are given for area 1 (d), 2 (e), and 3 (f) with the same outlines of the grains. The grains between 5 and 40 μm are generally well resolved; grains near the surface of the sample often show complex, nondipolar magnetic expressions that violate the assumptions of the inversion. Hence, they are not properly resolved (e.g., grain 1 in a and f).

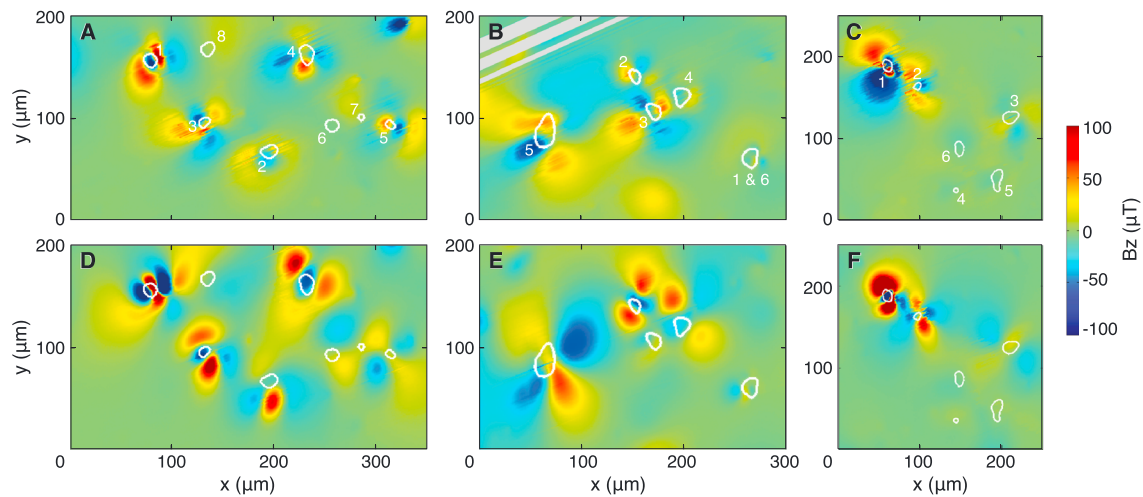


Figure 5. The differences between the scanning superconducting quantum interference device microscopy data (Figure 2) and the forward calculations based on the obtained magnetic moments per grain from the inversion (Figure 4). The results of area 1 (a), 2 (b), and 3 (c) of the sample in unknown magnetic state; the white outlines are the locations of the grains; the numbers refer to grains in the text and Table S2. The results for the sample in the an hysteretic remanent magnetization state are given for area 1 (d), 2 (e), and 3 (f) with the same outlines of the grains. The residuals for the deeper grains ($>5 \mu\text{m}$ from the surface) are generally low and nonuniform. For grains closer to the surface (e.g., grain 1 in panel d and grains 1 and 2 in panel f) the residuals are larger and more coherent, as the expression of their magnetization in the scanning superconducting quantum interference device microscopy violates our assumption of uniformly magnetized grains.

higher than the magnetic moment of a grain of $10 \mu\text{m}$ (Figure 3b). Our observations go beyond bulk measurements on carefully selected suites of grains (e.g., Dunlop & Özdemir, 1997; Hartstra, 1982) that until now define our knowledge of rock-magnetic behavior as function of grain sizes and shapes, chemistry, thermal history, and anisotropies and illustrate the potential of direct observations of magnetizations of individual particles for rock-magnetic research.

4. Discussion and Conclusions

The accuracy of the inversion is assessed by comparing the measured flux densities with the results of a forward model based on the spatial definitions of the grains and the inverted magnetic moments (Figure 4). Subtracting these forward calculations from the SSM data yields maps of residuals (Figure 5). Counterintuitively, grains $>5 \mu\text{m}$ from the surface of the sample show nonuniform and generally low residuals compared to the SSM signals, while the residuals for grains that are $<5 \mu\text{m}$ from the surface are often larger (e.g., Figures 2a/5a, grain 1; Figures 2f/5f, grain 1). Due to their close proximity to the surface, the magnetic expression of shallow grains may be dominated by their MD structure; these grains therefore violate our assumption to solve for a uniform dipolar magnetization per grain and are rejected. The inversion is insensitive to small perturbations in the mapping between the SSM and microCT data (Figures S4 and S5), further testifying to the uniqueness of the solution.

Obtaining the individual magnetizations of grains embedded in a medium nondestructively enables selecting the contribution from grains that are known reliable recorders and the rejection of grains that behave adversely. The Maxwell-Boltzmann limit for a meaningful statistical characterization of a paleomagnetic direction or intensity for typical paleomagnetic recorders is $>10^6$ magnetic particles (Berndt et al., 2016). To assess the feasibility of upscaling toward analyzing a natural sample, we made a microCT analysis of a volcanic sample (HW03, from de Groot et al., 2013). Surprisingly, selecting the proper attenuation contrast to isolate the iron oxides turned out to be easier than for our synthetic sample, possibly because the differences in density with respect to the surrounding grains are smaller; hence, adverse beam hardening effects are suppressed and boundaries are better defined.

The concentration of magnetic markers in the volcanic sample is ~ 20 times higher than in our synthetic sample ($\sim 72,000$ grains per cubic millimeter). With the surface to volume ratio of our $\sim 50 \mu\text{m}$ thick disk and a resolution of the SSM of $1 \mu\text{m}$, however, there still would be ~ 100 data points in the SSM scan per variable to solve, a vastly overdetermined system. Furthermore, an area of $<3 \text{ cm}^2$ would be enough to solve for

$>10^6$ grains; this is feasible in terms of magnetometry, leaving computer power for the inversion currently as main impediment to reach the Maxwell-Boltzmann limit and obtain meaningful paleomagnetic information from natural samples.

We are currently scanning at 4 K because the sample and the sensor of the SSM are together submerged in liquid helium; scanning at room temperature is necessary to obtain rock-magnetic information pertaining to the past state of the Earth's magnetic field. The SSM has unsurpassed sensitivity compared to other types of scanning magnetometry used in rock magnetism studies today, such as magnetic tunnel junction sensors and quantum diamond microscopes. The magnetic flux density at the surface of our synthetic sample, however, is already large enough to be properly measured by both these other techniques (with the normal component of the flux density varying between $\pm 100 \mu\text{T}$, at $\sim 2 \mu\text{m}$ above the surface). As the concentration of magnetic markers in a natural lava is much higher, the flux density at the surface is at least in the same order of magnitude but most likely much higher. Other scanning magnetometer techniques should therefore also be useful for our inversion technique, even with the larger sample-sensor distances associated with those techniques. Choosing the most suitable scanning magnetometer and optimizing the resolution of the microCT scanner will therefore help to unlock the statistical paleomagnetic information from even the smallest, and most challenging, rock-magnetic recorders such as the oldest igneous rocks and meteorites.

Acknowledgments

Ankur Rastogi is gratefully acknowledged for his help and advice in setting up the SSM equipment in the initial stage of the project. LvdG acknowledges NWO VENI grant 863.15.003. All authors declare no competing interests. The SSM and microCT data are available in PANGAEA: <https://doi.org/10.1594/PANGAEA.886724>.

References

- Almeida, T. P., Kasama, T., Muxworthy, A. R., Williams, W., Nagy, L., & Dunin-Borkowski, R. E. (2014). Observing thermomagnetic stability of nonideal magnetite particles: Good paleomagnetic recorders? *Geophysical Research Letters*, *41*, 7041–7047. <https://doi.org/10.1002/2014GL061432>
- Berndt, T., Muxworthy, A. R., & Fabian, K. (2016). Does size matter? Statistical limits of paleomagnetic field reconstruction from small rock specimens. *Journal of Geophysical Research: Solid Earth*, *121*, 15–26. <https://doi.org/10.1002/2015JB012441>
- Biggin, A. J., Piispa, E. J., Pesonen, L. J., Holme, R., Paterson, G. A., Veikkolainen, T., & Tauxe, L. (2015). Palaeomagnetic field intensity variations suggest Mesoproterozoic inner-core nucleation. *Nature*, *526*(7572), 245–248. <https://doi.org/10.1038/nature15523>
- de Groot, L. V., Biggin, A. J., Dekkers, M. J., Langereis, C. G., & Herrero-Bervera, E. (2013). Rapid regional perturbations to the recent global geomagnetic decay revealed by a new Hawaiian record. *Nature Communications*, *4*, 2727–2727. <https://doi.org/10.1038/ncomms3727>
- de Groot, L. V., Fabian, K., Bakelaar, I. A., & Dekkers, M. J. (2014). Magnetic force microscopy reveals meta-stable magnetic domain states that prevent reliable absolute palaeointensity experiments. *Nature Communications*, *5*, 5548. <https://doi.org/10.1038/ncomms5548>
- Dunlop, D. J., & Özdemir, Ö. (1997). *Cambridge studies in magnetism: Rock magnetism: Fundamentals and frontiers* (p. 573). Cambridge, UK: Cambridge University Press.
- Fabian, K. & de Groot, L. V. (2017). A uniqueness theorem in potential theory with implications for tomography-assisted inversion. arXiv:1712.06136v1 [physics.geo-ph]. Retrieved from <https://arxiv.org/abs/1712.06136>
- Farchi, E., Ebert, Y., Farfurnik, D., Haim, G., Shaar, R., & Bar-Gill, N. (2017). Quantitative vectorial magnetic imaging of multi-domain rock forming minerals using nitrogen-vacancy centers in diamond. *Spine*, *7*(03), 1740015. <https://doi.org/10.1142/S201032471740015X>
- Glenn, D. R., Fu, R. R., Kehayias, P., le Sage, D., Lima, E. A., Weiss, B. P., & Walsworth, R. L. (2017). Micrometer-scale magnetic imaging of geological samples using a quantum diamond microscope. *Geochemistry, Geophysics, Geosystems*, *18*(8), 3254–3267. <https://doi.org/10.1002/2017GC006946>
- Hartstra, R. L. (1982). Grain-size dependence of initial susceptibility and saturation magnetization-related parameters of four natural magnetites in the PSD—MD range. *Geophysical Journal of the Royal Astronomical Society*, *71*(2), 477–495. <https://doi.org/10.1111/j.1365-246X.1982.tb05998.x>
- Kirtley, J. R., & Wikswo, J. P. (1999). Scanning SQUID microscopy. *Annual Review of Materials Science*, *29*(1), 117–148. <https://doi.org/10.1146/annurev.matsci.29.1.117>
- Lima, E. A., Bruno, A. C., Carvalho, H. R., & Weiss, B. P. (2014). Scanning magnetic tunnel junction microscope for high-resolution imaging of remanent magnetization fields. *Measurement Science and Technology*, *25*(10), 105401–105415. <https://doi.org/10.1088/0957-0233/25/10/105401>
- Lima, E. A., & Weiss, B. P. (2009). Obtaining vector magnetic field maps from single-component measurements of geological samples. *Journal of Geophysical Research*, *114*, B06102. <https://doi.org/10.1029/2008JB006006>
- Muxworthy, A. R., Dunlop, D. J., & Özdemir, Ö. (2003). Low-temperature cycling of isothermal and anhysteretic remanence: Microcoercivity and magnetic memory. *Earth and Planetary Science Letters*, *205*(3–4), 173–184. [https://doi.org/10.1016/S0012-821X\(02\)01039-7](https://doi.org/10.1016/S0012-821X(02)01039-7)
- Muxworthy, A. R., & McClelland, E. (2000). The causes of low-temperature demagnetization of remanence in multidomain magnetite. *Geophysical Journal International*, *140*(1), 115–131. <https://doi.org/10.1046/j.1365-246x.2000.00000.x>
- Néel, L. (1949). Théorie du trainage magnétique des ferromagnétiques en grains fines avec applications aux terres cuites. *Annales de Géophysique*, *5*, 99–136.
- Néel, L. (1955). Some theoretical aspects of rock magnetism. *Advances in Physics*, *4*(14), 191–243. <https://doi.org/10.1080/00018735500101204>
- Nichols, C. I. O., Bryson, J. F. J., Herrero-Albillos, J., Kronast, F., Nimmo, F., & Harrison, R. J. (2016). Pallasite paleomagnetism: Quiescence of a core dynamo. *Earth and Planetary Science Letters*, *441*, 103–112.
- Sakellariou, A., Sawkins, T. J., Senden, T. J., & Limaye, A. (2004). X-ray tomography for mesoscale physics applications. *Physica A: Statistical Mechanics and its Applications*, *339*(1–2), 152–158. <https://doi.org/10.1016/j.physa.2004.03.055>
- Tarduno, J. A., Cottrell, R. D., Watkeys, M. K., Hofmann, A., Doubrovine, P. V., Mamajek, E. E., et al. (2010). Geodynamo, solar wind, and magnetopause 3.4 to 3.45 billion years ago. *Science*, *327*(5970), 1238–1240. <https://doi.org/10.1126/science.1183445>
- Weiss, B. P., Lima, E. A., Fong, L. E., & Baudenbacher, F. J. (2007). Paleomagnetic analysis using SQUID microscopy. *Journal of Geophysical Research*, *112*, B09105. <https://doi.org/10.1029/2007JB004940>